Dynamic responses of carbon nanotube-reinforced composite plates with surface-bonded piezoelectric sensor and actuator layers

*Chih-Ping Wu[1)] and Hong-Ru Lin[2)]

[1), 2)] *National Cheng Kung University, Taiwan, ROC*
[1)] cpwu@mail.ncku.edu.tw

ABSTRACT

A unified formulation of finite layer methods (FLMs) based on the Reissner mixed variational theorem (RMVT) is developed for the three-dimensional dynamic responses of simply-supported, functionally graded carbon nanotube-reinforced composite (CNTRC) plates with surface-bonded piezoelectric sensor and actuator layers and closed- and open-circuit surface conditions. In the formulation, the plate is divided into a number of finite rectangular layers, in which the trigonometric functions and Lagrange polynomials are used to interpolate the in- and out-of-plane variations of the primary field variables of each individual layer, respectively, such as the elastic displacement, transverse shear and normal stress, electric potential, and normal electric displacement (flux) components. The relevant orders used for expansion of these variables in the thickness coordinate can be freely chosen, such as linear, quadratic or cubic ones. Four different through-thickness distributions of carbon nanotubes in the CNTRC layer are considered, and the effective material properties of the layer are estimated using the rule of mixtures. The accuracy and convergence rate of the frequency parameters of the sandwiched hybrid CNTRC and piezoelectric plates obtained using assorted RMVT-based FLMs are assessed by comparing their solutions with the exact 3D solutions available in the literature.

1. INTRODUCTION

In recent decades, piezoelectric material layers have been either surface-bonded with or embedded in laminated fiber-reinforced composite (FRC) structures to produce so-called smart structures, and used as sensors and actuators to alter the structure's responses, due to the direct and reverse effects between the electric and elastic field variables.

Carbon nanotubes (CNT), with the characteristics of extraordinary specific stiffness and strength, have been mixed with polymer matrices to form the CNT-reinforced beam-, plate- and shell-like composite structures, and these have tremendous potential for various practical applications in the near future (Coleman et al., 2006; Ramaratnam and Jalili, 2006; Esai and Farag, 2007; Li et al., 2008). The analysis of CNT-reinforced composite (CNTRC) structures has thus attracted considerable research attention.

Based on the Reissner's mixed variation theorem (RMVT), Wu and Li (2010a, b) and Wu et al. (2013) developed unified formulations of the RMVT-based finite layer

methods (FLMs) for the static, vibration and stability analyses of simply-supported, multilayered FG elastic plates and laminated composite ones. Wu and Li (2013) further developed RMVT-based finite prism methods (FPMs) for the 3D analysis of laminated composite plates and multilayered FG elastic ones with various boundary conditions.

After a close literature survey, we found that there are relatively few articles that carry out the coupled analysis of sandwiched hybrid CNTRC and piezoelectric structures, as compared to those for conventional laminated hybrid FRC and piezoelectric ones. On the basis of 3D piezoelectricity, this article thus aims at developing RMVT-based FLMs for the dynamic responses of simply-supported, FG CNTRC plates with surface-bonded piezoelectric sensor and actuator layers and with closed- and open-circuit surface conditions. Four different through-thickness distributions of CNTs are considered, namely the UD, and FG V-, rhombus- (R-) and X-type ones, and the effective material properties of these FG CNTRC plates are evaluated using the rule of mixtures. A parametric study with regard to the effects of different CNT distributions, volume fractions of CNTs, aspect ratios, and thickness ratios for each layer on the frequency parameters and their corresponding modal electric and elastic variables of the sandwiched hybrid CNTRC and piezoelectric plates is also undertaken.

2. RMVT-BASED FINITE CYLINDRICAL PRISM METHODS

2.1. Carbon Nanotube-Reinforced Composite Layer

In this article, we consider the dynamic responses of simply-supported, either single-layered FG CNTRC or laminated FRC plates, combined with surface-bonded piezoelectric layers and with closed- and open-circuit surface conditions, as shown in Fig. 1a. A Cartesian global coordinate system (i.e., *x*, *y* and ζ coordinates) is located on the middle plane of the plate, and a set of Cartesian local thickness coordinates, $z_m\,(m=1,\,2,\,3,\cdots,\,N_l)$, is located at the mid-plane of each individual layer, as shown in Figs. 1b and 1c, in which N_l is the total number of the layers constituting the plate. The thicknesses of each individual layer and the plate are $h_m\ (m=1,2,\cdots,N_l)$ and *h*, respectively, while $h=\sum_{m=1}^{N_l} h_m$. L_x and L_y denote the in-plane dimensions in the *x* and *y* directions, respectively. The relationship between the global and local thickness coordinates in the m^{th}-layer is $\zeta=\bar{\zeta}_m+z_m$, in which $\bar{\zeta}_m=(\zeta_m+\zeta_{m-1})/2$, and ζ_m and ζ_{m-1} are the global thickness coordinates measured from the mid-plane of the plate to the top and bottom surfaces of the m^{th}-layer, respectively.

There are four different distribution functions of CNTs varying in the thickness direction of the FG CNTRC layer considered in this article, which are the UD, and the FG V-, R-, and X-type variations. The rule of mixtures is used to determine the through-thickness distributions of the effective material properties of the FG CNTRC layer, and these are written as follows:

$$E_{11}=\lambda_1 V_{CNT}\,(E_{11})_{CNT}+(V_m\,E_m)\,, \tag{1a}$$

$$\eta_{11}=\lambda_1 V_{CNT}\,(\eta_{11})_{CNT}+[V_m\,\eta_m]\,, \tag{1b}$$

$$\left(\lambda_2 / E_{22}\right)=V_{CNT} /\left(E_{22}\right)_{CNT}+\left(V_m / E_m\right), \tag{1c}$$

$$\left(\lambda_3 / G_{12}\right)=V_{CNT} /\left(G_{12}\right)_{CNT}+\left(V_m / G_m\right), \tag{1d}$$

$$\left(\lambda_2 / \eta_{kk}\right)=V_{CNT} /\left(\eta_{kk}\right)_{CNT}+\left(V_m / \eta_m\right) \quad (k=2 \text{ and } 3), \tag{1e}$$

in which $\left(E_{11}\right)_{CNT}$, $\left(E_{22}\right)_{CNT}$, $\left(G_{12}\right)_{CNT}$ and $\left(\eta_{kk}\right)_{CNT}$ (k=1-3) denote the Young's moduli, shear modulus and dielectric coefficients of CNTs; E_m, G_m and η_m stand for the corresponding properties of the polymer matrix; $\lambda_i \quad (i=1-3)$ are the CNT efficiency

(a)

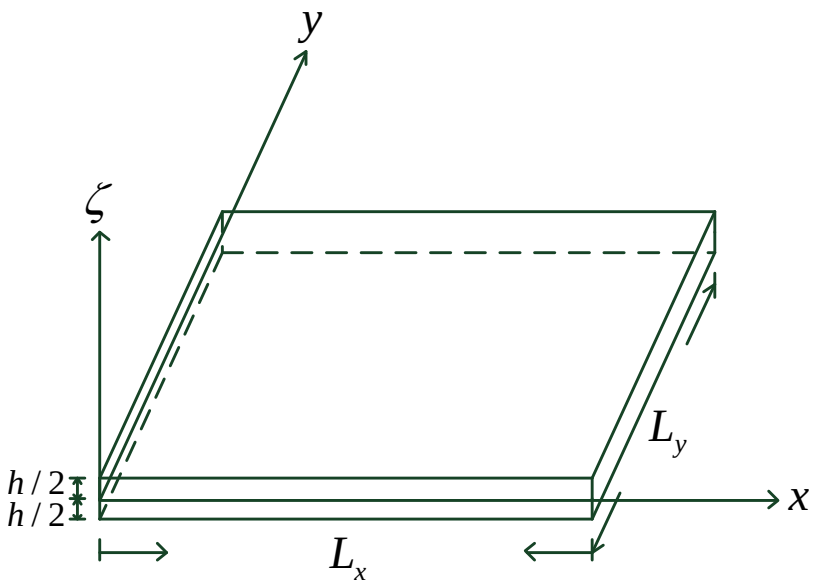

Fig.1(a) The configuration and coordinates of an FG piezoelectric plate

(b)

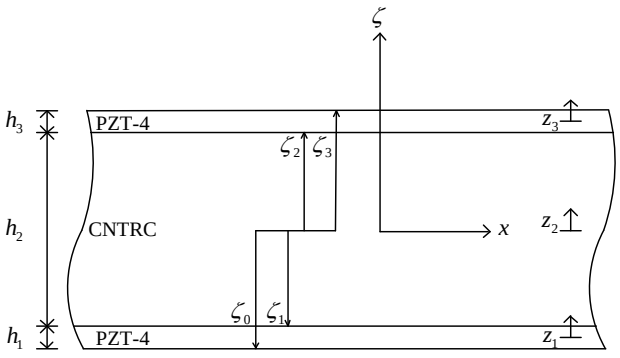

Fig.1(b) The layer stacking sequence and the local thickness coordinates of a sandwiched CNTRC and piezoelectric plate.

parameters, in which, for simplicity, $\lambda_2 = \lambda_3$ is assumed, and V_{CNT} and V_m are the volume fraction of CNTs and the polymer matrix, respectively, in which $V_{CNT} + V_m = 1$.The through-thickness distributions of the volume fraction of CNTs, V_{CNT} , for the above-mentioned four types of CNTRC plates are given as follows:

$$V_{CNT} = V_{CNT}^{*}, \quad \text{(UD-typed CNTRC layer),} \tag{2a}$$

$$V_{CNT}(\zeta) = \left[1 + (2\zeta / h_c)\right] V_{CNT}^{*} \quad \text{(FG V-typed CNTRC layer),} \tag{2b}$$

$$V_{CNT}(\zeta) = 2\left[1 - (2|\zeta| / h_c)\right] V_{CNT}^{*} \quad \text{(FG R-typed CNTRC layer),} \tag{2c}$$

$$V_{CNT}(\zeta) = 2(2|\zeta| / h_c)\, V_{CNT}^{*} \quad \text{(FG X-typed CNTRC layer),} \tag{2d}$$

in which V_{CNT}^{*} denotes the volume fraction index of CNTs, and is given as

$$V_{CNT}^{*} = W_{CNT} / [W_{CNT} + (\rho_{CNT} / \rho_m) - (\rho_{CNT} / \rho_m) W_{CNT}],$$

in which h_c denotes the thickness of the CNTRC layer, W_{CNT} denotes the mass fraction of CNTs in the CNTRC layer, and ρ_{CNT} and ρ_m are the mass densities of the CNT reinforcements and the polymer matrix, respectively.

Similarly, Poisson's ratio ν_{12} and the density ρ of the CNTRC layer are determined in the same way, as follows:

$$\upsilon_{12} = V_{CNT}^{*} (\nu_{12})_{CNT} + (V_m \nu_m), \tag{3a}$$

$$\rho = V_{CNT} \rho_{CNT} + V_m \rho_m, \tag{3b}$$

in which $(\nu_{12})_{CNT}$ and ν_m are Poisson's ratios of the CNT reinforcements and the polymer matrix, respectively, and ν_{12} is considered as a constant through the thickness coordinate of the CNTRC layer.

Using Eqs. (1a-e), (2a-d) and (3a, b), we can obtain the through-thickness distributions of the effective properties of CNTRC layer, which will be applied to the illustrative examples later in this article.

3. THE REISSNER MIXED VARIATIONAL THEOREM (RMVT)-BASED FLMs

3.1. Generalized Kinematic and Kinetic Assumptions

A unified formulation of RMVT-based FLMs is developed for the 3D free vibration analysis of sandwiched hybrid CNTRC (or FRC) and piezoelectric plates with closed- and open-circuit surface conditions. In this formulation, the plate is divided into a number of rectangular layers, and the elastic displacement and electric potential components of a typical layer (i.e., the m^{th}-layer) of the plate, for which the domain is in $0 \le x \le L_x$, $0 \le y \le L_y$ and $(-h_m/2) \le z_m \le (h_m/2)$, are given by

$$u_x^{(m)}(x, y, z_m, t) = \sum_{i=1}^{n_u+1} \left[\psi_u^{(m)}(z_m)\right]_i \left[u^{(m)}(x, y, t)\right]_i, \tag{4}$$

$$u_y^{(m)}(x,y,z_m,t)=\sum_{i=1}^{n_u+1}\left[\psi_u^{(m)}(z_m)\right]_i\left[v^{(m)}(x,y,t)\right]_i, \tag{5}$$

$$u_\zeta^{(m)}(x,y,z_m,t)=\sum_{i=1}^{n_w+1}\left[\psi_w^{(m)}(z_m)\right]_i\left[w^{(m)}(x,y,t)\right]_i, \tag{6}$$

$$\Phi^{(m)}(x,y,z_m,t)=\sum_{i=1}^{n_\phi+1}\left[\psi_\phi^{(m)}(z_m)\right]_i\left[\phi^{(m)}(x,y,t)\right]_i, \tag{7}$$

where t denotes the time variable, $\left(u^{(m)}\right)_i$, $\left(v^{(m)}\right)_i$, $\left(w^{(m)}\right)_i$ and $\left(\phi^{(m)}\right)_i$ are the elastic displacement and electric potential components at the i^{th}-nodal plane of the m^{th}-layer of the plate, $\left(\psi_u^{(m)}\right)_i$, $\left(\psi_w^{(m)}\right)_i$ and $\left(\psi_\phi^{(m)}\right)_i$ are the corresponding shape functions, and n_u, n_w and n_ϕ denote the related orders used for expansion of the in- and out-of-plane displacement and electric potential components, respectively.

The transverse shear stress, transverse normal stress and normal electric displacement (flux) components are also regarded as the primary variables in these RMVT-based FLMs, and are assumed to be as follows:

$$\tau_{x\zeta}^{(m)}(x,y,z_m,t)=\sum_{i=1}^{n_\tau+1}\left[\psi_\tau^{(m)}(z_m)\right]_i\left[\tau_{13}^{(m)}(x,y,t)\right]_i, \tag{8}$$

$$\tau_{y\zeta}^{(m)}(x,y,z_m,t)=\sum_{i=1}^{n_\tau+1}\left[\psi_\tau^{(m)}(z_m)\right]_i\left[\tau_{23}^{(m)}(x,y,t)\right]_i, \tag{9}$$

$$\sigma_\zeta^{(m)}(x,y,z_m,t)=\sum_{i=1}^{n_\sigma+1}\left[\psi_\sigma^{(m)}(z_m)\right]_i\left[\sigma_3^{(m)}(x,y,t)\right]_i, \tag{10}$$

$$D_\zeta^{(m)}(x,y,z_m,t)=\sum_{i=1}^{n_D+1}\left[\psi_D^{(m)}(z_m)\right]_i\left[D_3^{(m)}(x,y,t)\right]_i, \tag{11}$$

where $\left(\tau_{13}^{(m)}\right)_i$, $\left(\tau_{23}^{(m)}\right)_i$, $\left(\sigma_3^{(m)}\right)_i$ and $\left(D_3^{(m)}\right)_i$ are the transverse shear stress, transverse normal stress and normal electric displacement components at the i^{th}-nodal plane of the m^{th}-layer of the plate, and $\left(\psi_\tau^{(m)}\right)_i$, $\left(\psi_\sigma^{(m)}\right)_i$ and $\left(\psi_D^{(m)}\right)_i$ are the corresponding shape functions, and n_τ, n_σ and n_D denote the related orders used for expansion of the in- and out-of-plane displacement and electric potential components, respectively.

For a typical layer, the linear constitutive equations, which are valid for the orthotropic piezoelectric materials, are given by

$$\begin{Bmatrix}\sigma_x^{(m)}\\ \sigma_y^{(m)}\\ \sigma_\zeta^{(m)}\\ \tau_{y\zeta}^{(m)}\\ \tau_{x\zeta}^{(m)}\\ \tau_{xy}^{(m)}\end{Bmatrix}=\begin{bmatrix}c_{11}^{(m)} & c_{12}^{(m)} & c_{13}^{(m)} & 0 & 0 & 0\\ c_{12}^{(m)} & c_{22}^{(m)} & c_{23}^{(m)} & 0 & 0 & 0\\ c_{13}^{(m)} & c_{23}^{(m)} & c_{33}^{(m)} & 0 & 0 & 0\\ 0 & 0 & 0 & c_{44}^{(m)} & 0 & 0\\ 0 & 0 & 0 & 0 & c_{55}^{(m)} & 0\\ 0 & 0 & 0 & 0 & 0 & c_{66}^{(m)}\end{bmatrix}\begin{Bmatrix}\varepsilon_x^{(m)}\\ \varepsilon_y^{(m)}\\ \varepsilon_\zeta^{(m)}\\ \gamma_{y\zeta}^{(m)}\\ \gamma_{x\zeta}^{(m)}\\ \gamma_{xy}^{(m)}\end{Bmatrix}-\begin{bmatrix}0 & 0 & e_{31}^{(m)}\\ 0 & 0 & e_{32}^{(m)}\\ 0 & 0 & e_{33}^{(m)}\\ 0 & e_{24}^{(m)} & 0\\ e_{15}^{(m)} & 0 & 0\\ 0 & 0 & 0\end{bmatrix}\begin{Bmatrix}E_x^{(m)}\\ E_y^{(m)}\\ E_\zeta^{(m)}\end{Bmatrix}, \tag{12}$$

$$\begin{Bmatrix} D_x^{(m)} \\ D_y^{(m)} \\ D_\zeta^{(m)} \end{Bmatrix} = \begin{bmatrix} 0 & 0 & 0 & 0 & e_{15}^{(m)} & 0 \\ 0 & 0 & 0 & e_{24}^{(m)} & 0 & 0 \\ e_{31}^{(m)} & e_{32}^{(m)} & e_{33}^{(m)} & 0 & 0 & 0 \end{bmatrix} \begin{Bmatrix} \varepsilon_x^{(m)} \\ \varepsilon_y^{(m)} \\ \varepsilon_\zeta^{(m)} \\ \gamma_{y\zeta}^{(m)} \\ \gamma_{x\zeta}^{(m)} \\ \gamma_{xy}^{(m)} \end{Bmatrix} + \begin{bmatrix} \eta_{11}^{(m)} & 0 & 0 \\ 0 & \eta_{22}^{(m)} & 0 \\ 0 & 0 & \eta_{33}^{(m)} \end{bmatrix} \begin{Bmatrix} E_x^{(m)} \\ E_y^{(m)} \\ E_\zeta^{(m)} \end{Bmatrix}, \tag{13}$$

where $\sigma_x^{(m)}$, $\sigma_y^{(m)}, \cdots,$ and $\tau_{xy}^{(m)}$ are the stress components, $\varepsilon_x^{(m)}$, $\varepsilon_y^{(m)}, \cdots,$ and $\gamma_{xy}^{(m)}$ are the strain components, $D_x^{(m)}$, $D_y^{(m)}$ and $D_\zeta^{(m)}$ are the electric displacement components, and $E_x^{(m)}$, $E_y^{(m)}$ and $E_\zeta^{(m)}$ are the electric field ones. $c_{ij}^{(m)}$, $e_{kl}^{(m)}$ and $\eta_{ll}^{(m)}$ are the elastic, piezoelectric and dielectric permeability coefficients, respectively, which are constants through the thickness coordinate in the homogeneous piezoelectric/elastic layers, and variable through the thickness coordinate in the FG piezoelectric/elastic layers, while $e_{kl}^{(m)}$ rather than $\eta_{ll}^{(m)}$ are zero for an elastic layer, such as the CNTRC layer and FRC one.

The strain-displacement relations for each individual layer are given by

$$\varepsilon_x^{(m)} = \sum_{i=1}^{n_u+1} \left(\psi_u^{(m)}\right)_i u_i^{(m)}{}_{,x}, \tag{14}$$

$$\varepsilon_y^{(m)} = \sum_{i=1}^{n_u+1} \left(\psi_u^{(m)}\right)_i v_i^{(m)}{}_{,y}, \tag{15}$$

$$\varepsilon_\zeta^{(m)} = \sum_{i=1}^{n_w+1} D\left(\psi_w^{(m)}\right)_i w_i^{(m)}, \tag{16}$$

$$\gamma_{x\zeta}^{(m)} = \sum_{i=1}^{n_u+1} D\left(\psi_u^{(m)}\right)_i u_i^{(m)} + \sum_{i=1}^{n_w+1} \left(\psi_w^{(m)}\right)_i w_i^{(m)}{}_{,x}, \tag{17}$$

$$\gamma_{y\zeta}^{(m)} = \sum_{i=1}^{n_u+1} D\left(\psi_u^{(m)}\right)_i v_i^{(m)} + \sum_{i=1}^{n_w+1} \left(\psi_w^{(m)}\right)_i w_i^{(m)}{}_{,y}, \tag{18}$$

$$\gamma_{xy}^{(m)} = \sum_{i=1}^{n_u+1} \left(\psi_u^{(m)}\right)_i u_i^{(m)}{}_{,y} + \sum_{i=1}^{n_u+1} \left(\psi_u^{(m)}\right)_i v_i^{(m)}{}_{,x}, \tag{19}$$

where the commas denote partial differentiation with respect to the suffix variables, and $D\left(\psi_j^{(m)}\right)_i = d\left(\psi_j^{(m)}\right)_i / dz_m$, in which $j = u$ and w.

The electric field-electric potential relations for each individual layer are given by

$$E_x^{(m)} = -\sum_{i=1}^{n_\phi+1} \left(\psi_\phi^{(m)}\right)_i \phi_i^{(m)}{}_{,x}, \tag{20}$$

$$E_y^{(m)} = -\sum_{i=1}^{n_\phi+1} \left(\psi_\phi^{(m)}\right)_i \phi_i^{(m)}{}_{,y}, \tag{21}$$

$$E_\zeta^{(m)} = -\sum_{i=1}^{n_\phi+1} D\left(\psi_\phi^{(m)}\right)_i \phi_i^{(m)}. \tag{22}$$

3.2. *Hamilton's Principle*

The Hamilton principle is used to derive the Euler-Lagrange equations of the plate, and its corresponding energy functional for the plate is written in the form of

$$\mathrm{I}_R = \int_{t_1}^{t_2} \left(T - \Pi_R\right) dt \,, \tag{23}$$

where *t* denotes the time variable. *T* and Π_R are the kinetic and RMVT-based potential energies of the plate, and are given as follows:

$$T = \sum_{m=1}^{N_l} \int_{-h_m/2}^{h_m/2} \iint_{\Omega} \left(\rho^{(m)}/2\right)\left[\left(u_x^{(m)},_t\right)^2 + \left(u_y^{(m)},_t\right)^2 + \left(u_\zeta^{(m)},_t\right)^2\right] dx\, dy\, dz_m \,, \tag{24}$$

$$\begin{aligned}
\Pi_R = \sum_{m=1}^{N_l} \int_{-h_m/2}^{h_m/2} \iint_{\Omega} & \left[\sigma_x^{(m)}\,\varepsilon_x^{(m)} + \sigma_y^{(m)}\,\varepsilon_y^{(m)} + \sigma_\zeta^{(m)}\,\varepsilon_\zeta^{(m)} + \tau_{x\zeta}^{(m)}\gamma_{x\zeta}^{(m)} + \tau_{y\zeta}^{(m)}\gamma_{y\zeta}^{(m)} + \tau_{xy}^{(m)}\gamma_{xy}^{(m)}\right. \\
& \left. - D_x^{(m)}E_x^{(m)} - D_y^{(m)}E_y^{(m)} - D_\zeta^{(m)}E_\zeta^{(m)} - B\left(\sigma_{ij}^{(m)},\, D_k^{(m)}\right)\right] dx\, dy\, dz_m - \int_{\Omega^+} \bar{q}_k^{+} u_k^{(N_l)}\left(z_{N_l} = h_{N_l}/2\right) dx\, dy \\
& - \int_{\Omega^-} \bar{q}_k^{-} u_k^{(1)}\left(z_1 = -h_1/2\right) dx\, dy - \int_{\Omega^+} \bar{D}_\zeta^{+}\Phi\, dx\, dy - \int_{\Omega^-} \bar{D}_\zeta^{-}\Phi\, dx\, dy - \int_{\Omega^+} D_\zeta\left(\Phi - \bar{\Phi}^{+}\right) dx\, dy \\
& - \int_{\Omega^-} D_\zeta\left(\Phi - \bar{\Phi}^{-}\right) dx\, dy - \sum_{m=1}^{N_l} \int_{-h_m/2}^{h_m/2} \int_{\Gamma_\sigma} \left(\bar{t}_x^{(m)}\,u_x^{(m)} + \bar{t}_y^{(m)}\,u_y^{(m)} + \bar{t}_\zeta^{(m)}\,u_\zeta^{(m)}\right) d\Gamma\, dz_m \\
& - \sum_{m=1}^{N_l} \int_{-h_m/2}^{h_m/2} \int_{\Gamma_u} \left[\left(u_x^{(m)} - \bar{u}_x^{(m)}\right) t_x^{(m)} + \left(u_y^{(m)} - \bar{u}_y^{(m)}\right) t_y^{(m)} + \left(u_\zeta^{(m)} - \bar{u}_\zeta^{(m)}\right) t_\zeta^{(m)}\right] d\Gamma\, dz_m \\
& - \sum_{m=1}^{N_l} \int_{-h_m/2}^{h_m/2} \int_{\Gamma_D} \left(\bar{D}_n^{(m)}\,\Phi^{(m)}\right) d\Gamma\, dz_m - \sum_{m=1}^{N_l} \int_{-h_m/2}^{h_m/2} \int_{\Gamma_\Phi} D_n^{(m)}\left(\Phi^{(m)} - \bar{\Phi}^{(m)}\right) d\Gamma\, dz_m,
\end{aligned} \tag{25}$$

where Ω denotes the plate domain on the $x-y$ plane, and $\Omega^{\pm}$ denote the top surface ($\zeta = h/2$) and the bottom surface ($\zeta = -h/2$) of the plate, in which the transverse shear and normal stresses ($\bar{q}_k^{\pm}$, $k = x, y$ and ζ), and either electric potential ($\bar{\Phi}^{\pm}$) or normal electric displacement ($\bar{D}_\zeta^{\pm}$) are prescribed, and that all these prescribed variables are take to be zero for the dynamic analysis (i.e., free vibration one) of the plate. Γ_σ, Γ_u, Γ_D and Γ_Φ denote the portions of the edge boundary, where the surface traction, elastic displacement, electric potential and normal electric displacement components are prescribed, respectively (i.e., $t_i = \bar{t}_i$ and $u_i = \bar{u}_i$, in which *i*= *x*, *y* and ζ; $\Phi = \bar{\Phi}$; $D_n = \bar{D}_n$), and $B(\sigma_{ij}^{(m)}, D_k^{(m)})$ is the complementary density function of the *m*$^{\text{th}}$-layer.

In the formulation, we take the elastic displacement, transverse shear and normal stress, electric potential and normal electric displacement components to be the primary variables subject to variation. Using the generalized kinematic and kinetic assumptions given in Eqs. (4)-(11), and then performing integration by parts, we may express the first-order variation of the kinetic and RMVT-based potential energy functions as follows:

$$
\begin{aligned}
\delta\Pi_R = \iint_\Omega \sum_{m=1}^{N_l} \int_{-h_m/2}^{h_m/2} & \left\{ \left(\delta\boldsymbol{\varepsilon}_p^{(m)}\right)^T \boldsymbol{\sigma}_p^{(m)} + \left(\delta\boldsymbol{\varepsilon}_s^{(m)}\right)^T \boldsymbol{\sigma}_s^{(m)} + \delta\varepsilon_\zeta^{(m)}\, \sigma_\zeta^{(m)} + \left(\delta\boldsymbol{\sigma}_s^{(m)}\right)^T \left(\boldsymbol{\varepsilon}_s^{(m)} - \mathbf{S}_\sigma^{(m)} \boldsymbol{\sigma}_s^{(m)} - \mathbf{S}_e^{(m)} \mathbf{E}_s^{(m)}\right) \right. \\
& + \delta\sigma_\zeta^{(m)} \left[\varepsilon_\zeta^{(m)} - \overline{\eta}^{(m)}\, \sigma_\zeta^{(m)} + \left(\mathbf{Q}_a^{(m)}\right)^T \boldsymbol{\varepsilon}_p^{(m)} - \overline{e}^{(m)}\, D_\zeta^{(m)}\right] - \left(\delta\mathbf{E}_s^{(m)}\right)^T \mathbf{D}_s^{(m)} - \delta E_\zeta^{(m)}\, D_\zeta^{(m)} \\
& \left. - \delta D_\zeta^{(m)} \left[E_\zeta^{(m)} + \overline{e}^{(m)}\, \sigma_\zeta^{(m)} - \left(\mathbf{Q}_b^{(m)}\right)^T \boldsymbol{\varepsilon}_p^{(m)} - \overline{c}^{(m)}\, D_\zeta^{(m)}\right] \right\} dx\, dy\, dz_m \\
& - \sum_{m=1}^{N_l} \int_{-h_m/2}^{h_m/2} \int_{\Gamma_\sigma} \left(\bar{t}_x^{(m)}\, \delta u_x^{(m)} + \bar{t}_y^{(m)}\, \delta u_y^{(m)} + \bar{t}_\zeta^{(m)}\, \delta u_\zeta^{(m)}\right) d\Gamma\, dz_m - \sum_{m=1}^{N_l} \int_{-h_m/2}^{h_m/2} \int_{\Gamma_D} \left(\overline{D}_n^{(m)}\, \delta\Phi^{(m)}\right) d\Gamma\, dz_m \\
& - \sum_{m=1}^{N_l} \int_{-h_m/2}^{h_m/2} \int_{\Gamma_\phi} \left(\Phi^{(m)} - \overline{\Phi}^{(m)}\right) \delta D_n^{(m)} d\Gamma\, dz_m \\
& - \sum_{m=1}^{N_l} \int_{-h_m/2}^{h_m/2} \int_{\Gamma_u} \left[(u_x^{(m)} - \bar{u}_x^{(m)})\, \delta t_x^{(m)} + (u_y^{(m)} - \bar{u}_y^{(m)})\, \delta t_y^{(m)} + (u_\zeta^{(m)} - \bar{u}_\zeta^{(m)})\, \delta t_\zeta^{(m)}\right] d\Gamma\, dz_m,
\end{aligned}
\tag{26}
$$

$$
\delta T = -\iint_\Omega \sum_{m=1}^{N_l} \int_{-h_m/2}^{h_m/2} \rho^{(m)} \left[\left(\delta\mathbf{u}^{(m)}\right)^T \left(\mathbf{B}_{10}^{(m)}\right)^T \mathbf{B}_{10}^{(m)} \mathbf{u}^{(m)}{}_{,tt} + \rho^{(m)} \left(\delta\mathbf{w}^{(m)}\right)^T \left(\mathbf{B}_{11}^{(m)}\right)^T \mathbf{B}_{11}^{(m)} \mathbf{w}^{(m)}{}_{,tt}\right] dx\, dy\, dz_m \,, \tag{27}
$$

where the superscript of *T* denotes the transposition of the matrices or vectors, and Γ_u and Γ_σ stand for the boundary edges, in which the essential and natural conditions are prescribed.

$$
\boldsymbol{\varepsilon}_p^{(m)} = \left[\varepsilon_x^{(m)} \quad \varepsilon_y^{(m)} \quad \gamma_{xy}^{(m)}\right]^T = \mathbf{B}_1^{(m)}\, \mathbf{u}^{(m)}, \qquad \boldsymbol{\varepsilon}_s^{(m)} = \left[\gamma_{x\zeta}^{(m)} \quad \gamma_{y\zeta}^{(m)}\right]^T = \mathbf{B}_3^{(m)}\, \mathbf{u}^{(m)} + \mathbf{B}_4^{(m)}\, \mathbf{w}^{(m)},
$$

$$
\varepsilon_\zeta^{(m)} = \mathbf{B}_6^{(m)}\, \mathbf{w}^{(m)}, \qquad \boldsymbol{\sigma}_p^{(m)} = \left[\sigma_x^{(m)} \quad \sigma_y^{(m)} \quad \tau_{xy}^{(m)}\right]^T = \mathbf{Q}_p^{(m)}\, \mathbf{B}_1^{(m)}\, \mathbf{u}^{(m)} + \mathbf{Q}_a^{(m)}\, \mathbf{B}_2^{(m)}\, \boldsymbol{\sigma}^{(m)} + \mathbf{Q}_b^{(m)}\, \mathbf{B}_9^{(m)}\, \mathbf{D}^{(m)},
$$

$$
\boldsymbol{\sigma}_s^{(m)} = \left[\tau_{x\zeta}^{(m)} \quad \tau_{y\zeta}^{(m)}\right]^T = \mathbf{B}_5^{(m)}\, \boldsymbol{\tau}^{(m)}, \qquad \sigma_\zeta^{(m)} = \mathbf{B}_2^{(m)}\, \boldsymbol{\sigma}^{(m)}, \qquad \mathbf{E}_s^{(m)} = \left[E_x^{(m)} \quad E_y^{(m)}\right]^T = -\mathbf{B}_7^{(m)}\, \boldsymbol{\Phi}^{(m)},
$$

$$
E_\zeta^{(m)} = -\mathbf{B}_8^{(m)}\, \boldsymbol{\Phi}^{(m)}, \qquad \mathbf{D}_s^{(m)} = \left[D_x^{(m)} \quad D_y^{(m)}\right]^T = \mathbf{S}_e^{(m)}\, \mathbf{B}_5^{(m)} \tau^{(m)} + \mathbf{S}_\eta^{(m)}\, \mathbf{B}_7^{(m)} \Phi^{(m)}, \qquad D_\zeta^{(m)} = \mathbf{B}_9^{(m)}\, \mathbf{D}^{(m)},
$$

$$
\mathbf{u}^{(m)} = \begin{bmatrix} u_i^{(m)} \\ v_i^{(m)} \end{bmatrix}_{i=1,2,\cdots,n_u+1}, \quad \mathbf{w}^{(m)} = \left[w_i^{(m)}\right]_{i=1,2,\cdots,n_w+1}, \quad \boldsymbol{\tau}^{(m)} = \begin{bmatrix} \left(\tau_{13}^{(m)}\right)_i \\ \left(\tau_{23}^{(m)}\right)_i \end{bmatrix}_{i=1,2,\cdots,n_\tau+1}, \quad \boldsymbol{\sigma}^{(m)} = \left[\left(\sigma_3^{(m)}\right)_i\right]_{i=1,2,\cdots,n_\sigma+1},
$$

$$
\boldsymbol{\Phi}^{(m)} = \left[\Phi_i^{(m)}\right]_{i=1,2,\cdots,n_\phi+1}, \qquad \mathbf{D}^{(m)} = \left[\left(D_3^{(m)}\right)_i\right]_{i=1,2,\cdots,n_D+1},
$$

$$
\mathbf{S}_\sigma^{(m)} = \begin{bmatrix} \left(1/c_{55}^{(m)}\right) & 0 \\ 0 & \left(1/c_{44}^{(m)}\right) \end{bmatrix}, \qquad \mathbf{S}_e^{(m)} = \begin{bmatrix} \left(e_{15}^{(m)}/c_{55}^{(m)}\right) & 0 \\ 0 & \left(e_{24}^{(m)}/c_{44}^{(m)}\right) \end{bmatrix},
$$

$$
\mathbf{S}_\eta^{(m)} = \begin{bmatrix} \left(\eta_{11}^{(m)} + e_{15}^{(m)} e_{15}^{(m)}/c_{55}^{(m)}\right) & 0 \\ 0 & \left(\eta_{22}^{(m)} + e_{24}^{(m)} e_{24}^{(m)}/c_{44}^{(m)}\right) \end{bmatrix}, \qquad \mathbf{Q}_p^{(m)} = \begin{bmatrix} Q_{11}^{(m)} & Q_{12}^{(m)} & 0 \\ Q_{12}^{(m)} & Q_{22}^{(m)} & 0 \\ 0 & 0 & Q_{66}^{(m)} \end{bmatrix},
$$

$$
\mathbf{Q}_a^{(m)} = \begin{bmatrix} a_1^{(m)} \\ a_2^{(m)} \\ 0 \end{bmatrix}, \qquad \mathbf{Q}_b^{(m)} = \begin{bmatrix} b_1^{(m)} \\ b_2^{(m)} \\ 0 \end{bmatrix}, \qquad \mathbf{B}_1^{(m)} = \begin{bmatrix} \left(\psi_u^{(m)}\right)_i \partial_x & 0 \\ 0 & \left(\psi_u^{(m)}\right)_i \partial_y \\ \left(\psi_u^{(m)}\right)_i \partial_y & \left(\psi_u^{(m)}\right)_i \partial_x \end{bmatrix}_{i=1,2,\cdots,n_u+1},
$$

$$
\mathbf{B}_2^{(m)} = \left[\left(\psi_\sigma^{(m)}\right)_i\right]_{i=1,2,\cdots,n_\sigma+1}, \qquad \mathbf{B}_3^{(m)} = \begin{bmatrix} \left(D\psi_u^{(m)}\right)_i & 0 \\ 0 & \left(D\psi_u^{(m)}\right)_i \end{bmatrix}_{i=1,2,\cdots,n_u+1},
$$

$$\mathbf{B}_4^{(m)}=\begin{bmatrix}\left(\psi_w^{(m)}\right)_i\,\partial_x\\ \left(\psi_w^{(m)}\right)_i\,\partial_y\end{bmatrix}_{i=1,2,\cdots,n_w+1},\quad \mathbf{B}_5^{(m)}=\begin{bmatrix}\left(\psi_\tau^{(m)}\right)_i & 0\\ 0 & \left(\psi_\tau^{(m)}\right)_i\end{bmatrix}_{i=1,2,\cdots,n_\tau+1},\quad \mathbf{B}_6^{(m)}=\left[\left(D\psi_w^{(m)}\right)_i\right]_{i=1,2,\cdots,n_w+1},$$

$$\mathbf{B}_7^{(m)}=\begin{bmatrix}\left(\psi_\phi^{(m)}\right)_i\,\partial_x\\ \left(\psi_\phi^{(m)}\right)_i\,\partial_y\end{bmatrix}_{i=1,2,\cdots,n_\phi+1},\quad \mathbf{B}_8^{(m)}=\left[D\left(\psi_\phi^{(m)}\right)_i\right]_{i=1,2,\cdots,n_\phi+1},\quad \mathbf{B}_9^{(m)}=\left[\left(\psi_D^{(m)}\right)_i\right]_{i=1,2,\cdots,n_D+1},$$

$$\mathbf{B}_{10}^{(m)}=\begin{bmatrix}\left(\psi_u^{(m)}\right)_i & 0\\ 0 & \left(\psi_u^{(m)}\right)_i\end{bmatrix}_{i=1,2,\cdots,n_u+1},\quad \mathbf{B}_{11}^{(m)}=\left[\left(\psi_w^{(m)}\right)_i\right]_{i=1,2,\cdots,n_w+1},$$

$$a_i^{(m)}=\left(\eta_{3\,3}^{(m)}\,c_{i3}^{(m)}+e_{3\,3}^{(m)}\,e_{3i}^{(m)}\right)/\left(\eta_{3\,3}^{(m)}\,c_{3\,3}^{(m)}+e_{3\,3}^{(m)}\,e_{3\,3}^{(m)}\right),\quad b_i^{(m)}=\left(e_{33}^{(m)}\,c_{i3}^{(m)}-e_{3i}^{(m)}\,c_{33}^{(m)}\right)/\left(\eta_{33}^{(m)}\,c_{33}^{(m)}+e_{33}^{(m)}\,e_{33}^{(m)}\right),$$

$$\bar{c}^{(m)}=c_{33}^{(m)}/\left(\eta_{33}^{(m)}\,c_{33}^{(m)}+e_{33}^{(m)}\,e_{33}^{(m)}\right),\quad \bar{e}^{(m)}=e_{33}^{(m)}/\left(\eta_{33}^{(m)}\,c_{33}^{(m)}+e_{33}^{(m)}\,e_{33}^{(m)}\right),\quad \bar{\eta}^{(m)}=\eta_{33}^{(m)}/\left(\eta_{33}^{(m)}\,c_{33}^{(m)}+e_{33}^{(m)}\,e_{33}^{(m)}\right),$$

$Q_{ij}^{(m)}=c_{ij}^{(m)}-a_j^{(m)}c_{i3}^{(m)}-b_j^{(m)}\,e_{3i}^{(m)}$ (*I, j*=1 and 2), and $Q_{66}^{(m)}=c_{66}^{(m)}$.

3.3. Euler–Lagrange Equations

The free vibration of simply-supported, sandwiched hybrid CNTRC and piezoelectric plates and laminated hybrid FRC and piezoelectric ones with closed- and open-circuit surface conditions is studied in the following illustrative examples. The boundary conditions on the lateral surfaces of the plates are given as follows:

Case 1. Closed-circuit surface conditions in which the mechanical traction loads and electric potential component are prescribed, with

$$\left[\tau_{x\zeta}^{(N_l)}(x,y,h/2)\quad \tau_{y\zeta}^{(N_l)}(x,y,h/2)\quad \sigma_\zeta^{(N_l)}(x,y,h/2)\quad \Phi^{(N_l)}(x,y,h/2)\right]=\left[0\quad 0\quad 0\quad 0\right]\quad \text{on the top surface,}\quad (28a)$$

$$\left[\tau_{x\zeta}^{(1)}(x,y,-h/2)\quad \tau_{y\zeta}^{(1)}(x,y,-h/2)\quad \sigma_\zeta^{(1)}(x,y,-h/2)\quad \Phi^{(1)}(x,y,-h/2)\right]=\left[0\quad 0\quad 0\quad 0\right]\quad \text{on the bottom surface.}\quad (28b)$$

Case 2. Open-circular surface conditions in which the mechanical traction loads and normal electric displacement component are prescribed, with

$$\left[\tau_{x\zeta}^{(N_l)}(x,y,h/2)\quad \tau_{y\zeta}^{(N_l)}(x,y,h/2)\quad \sigma_\zeta^{(N_l)}(x,y,h/2)\quad D_\zeta^{(N_l)}(x,y,h/2)\right]=\left[0\quad 0\quad 0\quad 0\right]\quad \text{on the top surface,}\quad (29a)$$

$$\left[\tau_{x\zeta}^{(1)}(x,y,-h/2)\quad \tau_{y\zeta}^{(1)}(x,y,-h/2)\quad \sigma_\zeta^{(1)}(x,y,-h/2)\quad D_\zeta^{(1)}(x,y,-h/2)\right]=\left[0\quad 0\quad 0\quad 0\right],\quad \text{on the bottom surface.}\quad (29b)$$

The edge conditions of each individual layer are considered as fully simple supports with free electric potentials, which requires that the following quantities are satisfied.

$$u_y^{(m)}=u_\zeta^{(m)}=\sigma_x^{(m)}=\Phi^{(m)}=0\quad \text{at}\quad x=0,\quad x=L_x\quad \text{and}\quad m=1,2,\cdots,N_l,\quad (30a)$$

$$u_x^{(m)}=u_\zeta^{(m)}=\sigma_y^{(m)}=\Phi^{(m)}=0\quad \text{at}\quad y=0,\quad y=L_y\quad \text{and}\quad m=1,2,\cdots,N_l.\quad (30b)$$

By means of the separation of variables, the primary field variables of each individual layer are expanded as the following forms of a double Fourier series so that

the boundary conditions of the simply supported edges are exactly satisfied. These are given as

$$\left(u_x^{(m)},\ \tau_{x\zeta}^{(m)}\right)=\sum_{m=1}^{\infty}\sum_{n=1}^{\infty}\left(u_{\hat{m}\hat{n}}^{(m)},\ \ \tau_{13\hat{m}\hat{n}}^{(m)}\right)\cos\tilde{m}x\ \sin\tilde{n}y\,e^{i\omega t}, \tag{31}$$

$$\left(u_y^{(m)},\ \tau_{y\zeta}^{(m)}\right)=\sum_{m=1}^{\infty}\sum_{n=1}^{\infty}\left(v_{\hat{m}\hat{n}}^{(m)},\ \ \tau_{23\hat{m}\hat{n}}^{(m)}\right)\sin\tilde{m}x\ \cos\tilde{n}y\,e^{i\omega t}, \tag{32}$$

$$\left(u_\zeta^{(m)},\ \sigma_\zeta^{(m)},\ \Phi^{(m)},\ D_\zeta^{(m)}\right)=\sum_{m=1}^{\infty}\sum_{n=1}^{\infty}\left(w_{\hat{m}\hat{n}}^{(m)},\ \sigma_{13\hat{m}\hat{n}}^{(m)},\ \phi_{\hat{m}\hat{n}}^{(m)},\ D_{3\hat{m}\hat{n}}^{(m)}\right)\sin\tilde{m}x\ \sin\tilde{n}y\,e^{i\omega t}, \tag{33}$$

where ω denotes the frequency of the natural vibration of the plate, and $\tilde{m}=\hat{m}\pi/L_x$ and $\tilde{n}=\hat{n}\pi/L_y$, in which $\hat{m}$ and $\hat{n}$ are the wave numbers in the *x* and *y* directions, respectively, and are positive intergers.

After introducing Eqs. (31)–(33) in Eq. (23) and using the Hamilton principle (i.e., $\delta I_R=0$), we obtain the Euler–Lagrange equations of the plate, as follows:

$$\sum_{m=1}^{N_l}\left\{\begin{bmatrix}\mathbf{K}_{\mathrm{I\ I}}^{(m)} & \mathbf{0} & \mathbf{K}_{\mathrm{I\ III}}^{(m)} & \mathbf{K}_{\mathrm{I\ IV}}^{(m)} & \mathbf{K}_{\mathrm{I\ V}}^{(m)} & \mathbf{0}\\ \mathbf{0} & \mathbf{0} & \mathbf{K}_{\mathrm{II\ III}}^{(m)} & \mathbf{K}_{\mathrm{II\ IV}}^{(m)} & \mathbf{0} & \mathbf{0}\\ \mathbf{K}_{\mathrm{III\ I}}^{(m)} & \mathbf{K}_{\mathrm{III\ II}}^{(m)} & \mathbf{K}_{\mathrm{III\ III}}^{(m)} & 0 & 0 & \mathbf{K}_{\mathrm{III\ VI}}^{(m)}\\ \mathbf{K}_{\mathrm{IV\ I}}^{(m)} & \mathbf{K}_{\mathrm{IV\ II}}^{(m)} & 0 & \mathbf{K}_{\mathrm{IV\ IV}}^{(m)} & \mathbf{K}_{\mathrm{IV\ V}}^{(m)} & 0\\ \mathbf{K}_{\mathrm{V\ I}}^{(m)} & 0 & 0 & \mathbf{K}_{\mathrm{V\ IV}}^{(m)} & \mathbf{K}_{\mathrm{V\ V}}^{(m)} & \mathbf{K}_{\mathrm{V\ VI}}^{(m)}\\ 0 & 0 & \mathbf{K}_{\mathrm{VI\ III}}^{(m)} & 0 & \mathbf{K}_{\mathrm{VI\ V}}^{(m)} & \mathbf{K}_{\mathrm{VI\ VI}}^{(m)}\end{bmatrix}-\omega^2\begin{bmatrix}\mathbf{M}_{\mathrm{I\ I}}^{(m)} & \mathbf{0} & \mathbf{0} & \mathbf{0} & \mathbf{0} & \mathbf{0}\\ \mathbf{0} & \mathbf{M}_{\mathrm{II\ II}}^{(m)} & \mathbf{0} & \mathbf{0} & \mathbf{0} & \mathbf{0}\\ \mathbf{0} & \mathbf{0} & \mathbf{0} & \mathbf{0} & \mathbf{0} & \mathbf{0}\\ \mathbf{0} & \mathbf{0} & \mathbf{0} & \mathbf{0} & \mathbf{0} & \mathbf{0}\\ \mathbf{0} & \mathbf{0} & \mathbf{0} & \mathbf{0} & \mathbf{0} & \mathbf{0}\\ \mathbf{0} & \mathbf{0} & \mathbf{0} & \mathbf{0} & \mathbf{0} & \mathbf{0}\end{bmatrix}\right\}\begin{bmatrix}\tilde{\mathbf{u}}^{(m)}\\ \tilde{\mathbf{w}}^{(m)}\\ \tilde{\boldsymbol{\tau}}^{(m)}\\ \tilde{\boldsymbol{\sigma}}^{(m)}\\ \tilde{\mathbf{D}}^{(m)}\\ \tilde{\Phi}^{(m)}\end{bmatrix}=\begin{bmatrix}\mathbf{0}\\ \mathbf{0}\\ \mathbf{0}\\ \mathbf{0}\\ \mathbf{0}\\ \mathbf{0}\end{bmatrix}, \tag{34}$$

where $\mathbf{K}_{i\ j}^{(m)}=\left(\mathbf{K}_{j\ i}^{(m)}\right)^T$ ($i,j=$ I, II, III, IV, V, VI), and the detailed expressions of $\mathbf{K}_{i\ j}^{(m)}$ are omitted.

After using Eq. (34) and assembling the local stiffness and mass matrices of each layer constituting the plate by following the standard process of the FEMs, in which the elastic displacement, transverse stress, electric potential and normal electric displacement continuity conditions at the interfaces between adjacent layers are imposed, and thus satisfied a priori, for the RMVT-based FLMs, we may construct the global stiffness and mass matrices for the plate. By solving the resulting system equations, the natural frequencies and their corresponding modal variables for a certain vibration mode $(\hat{m},\ \hat{n})$ can then be determined.

4. ILLUSTRATIVE EXAMPLES

A unified formulation of RMVT-based FLMs was derived above for the dynamic responses of simply-supported, multilayered hybrid elastic and piezoelectric plates, in which various combinations of the orders used for expansion of elastic displacement, transverse stress, electric potential and normal electric displacement components can be freely chosen, and the acronym, $\mathrm{LM}_{n_u\ n_w\ n_\phi}^{n_\tau\ n_\sigma\ n_D}$, is thus defined to represent various RMVT-based FLMs, in which the in-, out-of-plane elastic displacement and electric potential components are expanded as the n_u -, n_w - and n_ϕ -order Lagrange

polynomials in the thickness coordinate of each layer, respectively, while the transverse shear, normal stress and normal electric displacement components are expanded as the n_τ-, n_σ- and n_D-order Lagrange polynomials in this. In addition, an *h*-refinement process is adopted for this analysis, and the values of n_i $(i = u,\ w,\ \phi,\ \tau,\ \sigma \text{ and } D)$ are thus taken as 1, 2 and 3 in the following examples.

4.1. Single-layered FG CNTRC plates

In this section, we present the free vibration analysis of simply-supported, single-layered FG CNTRC plates, in which four different distributions of CNTs varying along the thickness coordinate (i.e., UD-, FG V-, R-, and X-type distributions) are considered. Polymer material PmPV is considered as the matrix, and CNTs are the reinforcements, the material properties of which are given in Table 1. The CNT efficiency parameters are taken as $\lambda_1 = 0.149$, $\lambda_2 = \lambda_3 = 0.934$ for the case of $V_{CNT}^* = 0.11$, $\lambda_1 = 0.150$, $\lambda_2 = \lambda_3 = 0.941$ for the case of $V_{CNT}^* = 0.14$, and $\lambda_1 = 0.149$, $\lambda_2 = \lambda_3 = 1.381$ for the case of $V_{CNT}^* = 0.17$. The effective material properties of these single-layered CNTRC plates through the thickness coordinate for different distributions of CNTs can be estimated using Eqs. (1)-(3). In addition, the dimensionless frequency parameter Ω is defined as $\Omega = \left(\omega L_x^2 / h\right)\sqrt{\rho_m / E_m}$.

Table 2 shows the ten-and twenty-layer LM_{22}^{22} and LM_{33}^{33} solutions for the frequency parameters of simply-supported, square FG CNTRC plates with different CNT distributions and vibration modes, in which the wave numbers ($\hat{m},\ \hat{n}$) are taken to be (1, 1), (1, 2), (1, 3), (1, 4), (2, 1) and (2, 2), $L_x / h = 50$, and V_{CNT}^* =0.14. It can be seen in Table 4 that the LM_{22}^{22} and LM_{33}^{33} solutions of the frequency parameters converge rapidly, and the relative solutions of twenty-layer LM_{22}^{22} and ten-layer LM_{33}^{33} are identical to the exact 3D solutions (Wu and Lu, 2009) with a four-digit decimal fraction, and that the lowest frequency parameter of the plate with a certain CNT distribution always occurs at ($\hat{m},\ \hat{n}$)=(1, 1). The convergent solutions of LM_{22}^{22} and LM_{33}^{33} also closely agree with the solutions obtained using the FSDT-based FEM by Zhu et al. (2012) and the ANSYS software. The magnitude order of the frequency parameters for the cases of UD- and FG R-, V- and X-type CNT distributions are FG X- > UD- > FG V- > FG R-type, which reflects the fact that CNT reinforcements distributed close to the top and bottom surfaces are more efficient than those distributed near the mid-surface with regard to enhancing the overall stiffness of the CNTRC plate, and this is also found in Zhu et al. (2012).

4.2. Sandwiched hybrid CNTRC and piezoelectric plates

In this section, we present the free vibration analysis of simply-supported, FG CNTRC plates with surface-bonded piezoelectric actuator and sensor layers and with open- and closed-circuit surface conditions (i.e., [PZT-4/CNTRC-layer/PZT-4] plates).

Figures 2 and 3 show the LM_{333}^{333} solutions for the through-thickness distributions of various modal elastic and electric variables of a sandwiched FG CNTRC and piezoelectric plates ($[\mathrm{PZT-4/CNTRC/PZT-4}]$) with closed- and open-circuit surface

Table 1
Elastic, piezoelectric and dielectric coefficients of composite and piezoelectric materials.

Moduli	PZT-4 (Heyliger and Saravanos, 1995)	SWCNT (300^0K) (Zhu et al., 2012)	PmPV matrix (Zhu et al., 2012)
E_{11} (Gpa)	81.3	5646.6	2.1
E_{22} (Gpa)	81.3	7080.0	2.1
E_{33} (Gpa)	64.5	7080.0	2.1
ν_{12}	0.329	0.175	0.34
ν_{13}	0.432	0.175	0.34
ν_{23}	0.432	0.175	0.34
G_{23} (Gpa)	25.6	1944.5	0.7836
G_{13} (Gpa)	25.6	1944.5	0.7836
G_{12} (Gpa)	30.6	1944.5	0.7836
e_{24} $(\mathrm{C/m^2})$	12.72	0.0	0.0
e_{15} $(\mathrm{C/m^2})$	12.72	0.0	0.0
e_{31} $(\mathrm{C/m^2})$	-5.2	0.0	0.0
e_{32} $(\mathrm{C/m^2})$	-5.2	0.0	0.0
e_{33} $(\mathrm{C/m^2})$	15.08	0.0	0.0
η_{11}/η_0 $(\mathrm{F/m})$	1475	2000	10
η_{22}/η_0 $(\mathrm{F/m})$	1475	2000	10
η_{33}/η_0 $(\mathrm{F/m})$	1300	2000	10
ρ $(\mathrm{Kg/m^3})$	7600	1400	1150

η_0 denotes the dielectric permittivity of free space, and η_0 =8.854e-12 (F/m)

conditions, respectively, in which $V^*_{CNT} = 0.14$, $L_x / L_y = 1$, $h_1 : h_2 : h_3 = 0.1h : 0.8h : 0.1h$, $(\hat{m},\ \hat{n}) = (1,\ 1)$, $(N_p,\ N_e) = (6,\ 24)$, L_x / h = 10, and that four different CNT distributions (i.e., UD, FG V-, R- and X-type) through the thickness coordinate of the CNTRC layer (core)

are considered. It can be seen from Figs. 4 and 5 that variations of elastic and electric modal variables appear to be linear and higher-order polynomials, respectively, along the thickness coordinate of the piezoelectric layer (face sheets), while these appear to be higher-order polynomials along the FG CNTRC layer (core). The different CNT distributions affect the through-thickness distributions of modal variables induced in the CNTRC layer (core) more significantly than those in the piezoelectric layers (face sheets). Again, it is shown that the prescribed traction loads and open- and closed-circuit conditions on the top and bottom surfaces, as well as the transverse

Table 2

The FLM solutions of the frequency parameters for square single-layered FG CNTRC plates with different CNT distributions and vibration modes $(L_x / h = 50)$.

$(\hat{m},\ \hat{n})$	Theories	UD	FG V-type	FG R-type	FG X-type
(1, 1)	LM_{22}^{22} $(N_l = 10)$	21.31669	17.94233	15.76275	25.49276
	LM_{22}^{22} $(N_l = 20)$	21.31668	17.94232	15.76276	25.49274
	LM_{33}^{33} $(N_l = 10)$	21.31668	17.94231	15.76274	25.49274
	LM_{33}^{33} $(N_l = 20)$	21.31668	17.94231	15.76276	25.49275
	Zhu et al. (2012)	21.354	17.995	15.801	25.555
	ANSYS (Zhu et al., 2012)	21.311	17.956	15.788	25.474
	Modified Pagano (Wu and Lu, 2009)	21.31668	17.94678	15.77889	25.48327
(1, 2)	LM_{22}^{22} $(N_l = 10)$	25.18789	22.53327	20.47672	29.04425
	LM_{22}^{22} $(N_l = 20)$	25.18788	22.53325	20.47688	29.04424
	LM_{33}^{33} $(N_l = 10)$	25.18788	22.53323	20.47671	29.04424
	LM_{33}^{33} $(N_l = 20)$	25.18788	22.53324	20.47688	29.04424
	Zhu et al. (2012)	25.295	22.643	20.563	29.192
	ANSYS (Zhu et al., 2012)	25.192	22.531	20.469	29.065
	Modified Pagano (Wu and Lu, 2009)	25.18788	22.53430	20.48464	29.03525
(2, 1)	LM_{22}^{22} $(N_l = 10)$	77.38969	65.52419	57.82381	90.40442
	LM_{22}^{22} $(N_l = 20)$	77.38957	65.52408	57.82375	90.40421
	LM_{33}^{33} $(N_l = 10)$	77.38956	65.52407	57.82373	90.40420
	LM_{33}^{33} $(N_l = 20)$	77.38956	65.52407	57.82375	90.40420
	Zhu et al. (2012)	78.110	66.552	58.748	87.814
	ANSYS (Zhu et al., 2012)	77.629	65.893	58.237	82.437
	Modified Pagano (Wu and Lu, 2009)	77.38956	65.54208	57.88751	90.37500
(2, 2)	LM_{22}^{22} $(N_l = 10)$	79.32286	67.94973	60.39849	92.09892
	LM_{22}^{22} $(N_l = 20)$	79.32274	67.94961	60.39850	92.09871
	LM_{33}^{33} $(N_l = 10)$	79.32273	67.94960	60.39841	92.09870
	LM_{33}^{33} $(N_l = 20)$	79.32273	67.94960	60.39849	92.09870
	Zhu et al. (2012)	80.015	68.940	61.277	91.299
	ANSYS (Zhu et al., 2012)	79.482	68.315	60.782	90.389
	Modified Pagano (Wu and Lu, 2009)	79.32273	67.96579	60.45715	92.06989

stress, electric potential and electric normal displacement continuity conditions at the interfaces between the face sheets and core, are exactly satisfied.

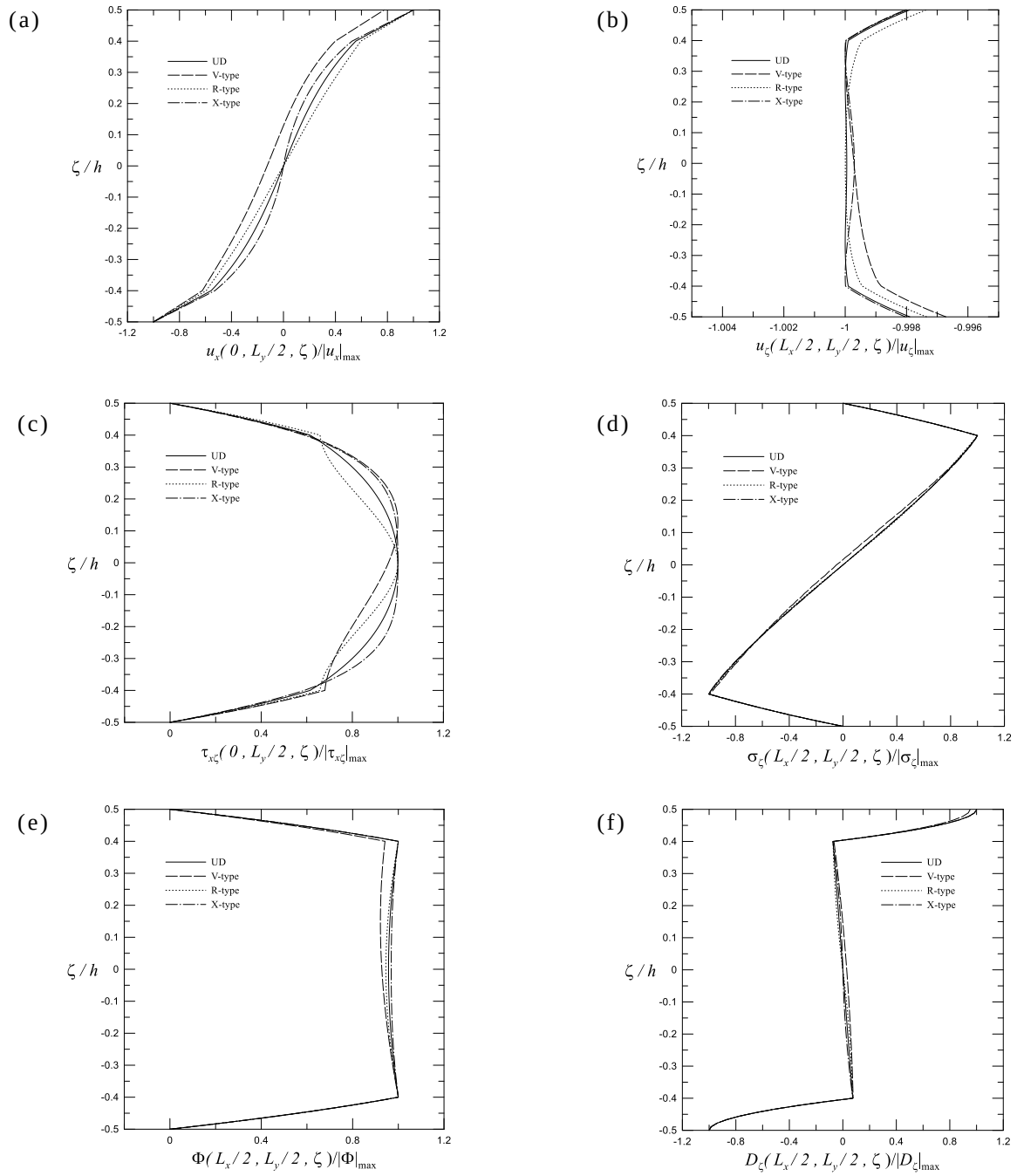

Fig. 4 The through-thickness distributions of various electric and elastic modal variables induced in a sandwiched CNTRC and piezoelectric plate ($[\mathrm{PZT-4/CNTRC/PZT\text{-}4}]$) with closed-circuit surface conditions and different CNT distributions.

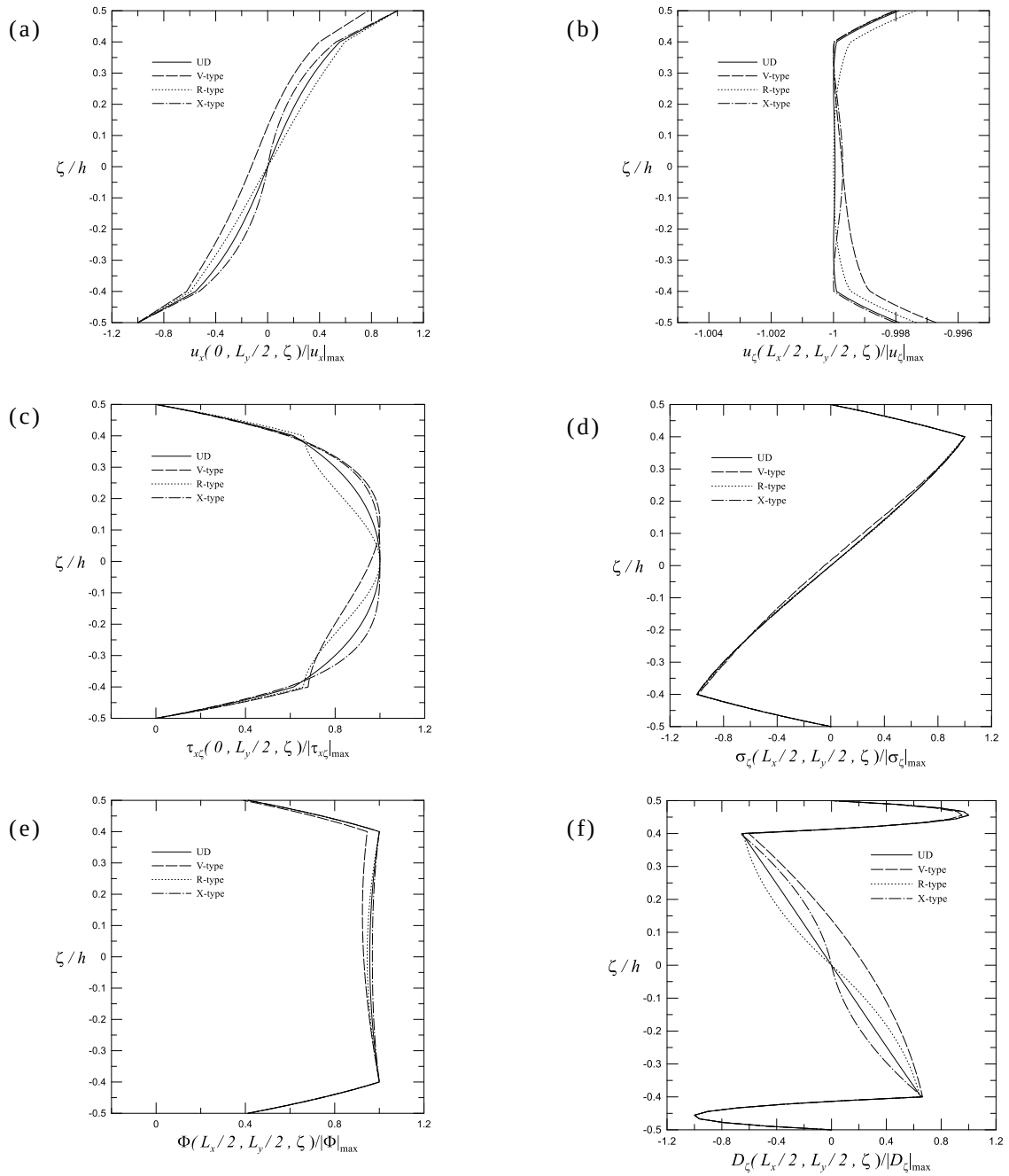

Fig. 5 The through-thickness distributions of various electric and elastic modal variables induced in a sandwiched CNTRC and piezoelectric plate ($[\text{PZT}-4/\text{CNTRC}/\text{PZT}-4]$) with open-circuit surface conditions and different CNT distributions.

5. CONCLUDING REMARKS

In this work, we developed a unified formulation of various RMVT-based FLMs to investigate the dynamic responses of simply supported, sandwiched hybrid CNTRC

and piezoelectric plates and multilayered hybrid FRC and piezoelectric ones with closed- and open-circuit surface conditions. The relative orders used for expansion of the displacement, transverse stress, electric potential and normal electric displacement components are suggested to be identical to one another. In the implementation of various RMVT-based FLMs with the *h*-refinement process, we found that the solutions of LM_{222}^{222} and LM_{333}^{333} converge rapidly when compared with the exact 3D piezoelectricity solutions available in the literature. The frequency parameters and the corresponding through-thickness distributions of the electric and elastic modal variables of the sandwiched hybrid CNTRC and piezoelectric plates were obtained. The results show that the frequency parameters increase when the volume fraction index of CNTs and the thickness of CNTRC layer become greater, and the frequency parameters for open-circuit surface conditions are slightly larger than those for closed-circuit surface ones. The magnitude order of the frequency parameters for the cases of UD- and FG R-, V- and X-type CNT distributions are FG X- > UD- > FG V- > FG R-type CNT ones.

ACKNOWLEDGMENTS

This work was supported by the National Science Council of Republic of China, through grant NSC 100-2221-E-006-180-MY3.

REFERENCES

Coleman, J.N., Khan, U., Blau, W.J. and Gun'ko, Y.K. (2006), "Small but strong: A review of the mechanical properties of carbon nanotube-polymer composites," *Carbon*, **44**, 1624-1652.

Esawi, A.M.K. and Farag, M.M. (2007), "Carbon nanotube reinforced composites: Potential and current challenges," Mater. Des., **28**, 2394-2401.

Li, C., Thostenson, E.T. and Chou, T.W. (2008) "Sensors and actuators based on carbon nanotubes and their composites: A review," *Compos. Sci. Technol.* **68**, 1227-1249.

Ramaratnam, A. and Jalili, N. (2006), "Reinforcement of piezoelectric polymers with carbon nanotubes: Pathway to next-generation sensors," *J. Intell. Mater. Sys. Struct*. **17**, 199-208.

Wu, C.P., Chen, Y.C. and Peng, S.T. (2013), "Buckling analysis of functionally graded material circular hollow cylinders under combined axial compression and external pressure," *Thin-Walled Struct*., **69**, 54-66.

Wu, C.P. and Li, H.Y. (2010a), "The RMVT- and PVD-based finite layer methods for the three-dimensional analysis of multilayered composite and FGM plates," *Compos. Struct.*, **92**, 2476-2496.

Wu, C.P. and Li, H.Y. (2010b), "RMVT- and PVD-based finite layer methods for the quasi-3D free vibration analysis of multilayered composite and FGM plates," *CMC-Comput. Mater. Continua*, **19**, 155-198.

Wu, C.P. and Li, H.Y. (2013), "An RMVT-based finite rectangular prism method for the 3D analysis of sandwich FGM plates with various boundary conditions," *CMC-Comput. Mater. Continua*, **34**, 27-62.